

## Binary reaction decays from $^{24}\text{Mg} + ^{12}\text{C}$

C. Beck,<sup>1,\*</sup> P. Papka,<sup>1,+</sup> A. Sánchez i Zafra,<sup>1</sup> S. Thummerer,<sup>1,2</sup> F. Azaiez,<sup>1,\*\*</sup>  
 P. Bednarczyk,<sup>1</sup> S. Courtin,<sup>1</sup> D. Curien,<sup>1</sup> O. Dorvaux,<sup>1</sup> D. Lebhertz,<sup>1</sup>  
 A. Nourreddine,<sup>1</sup> M. Rousseau,<sup>1</sup> W. von Oertzen,<sup>2</sup> B. Gebauer,<sup>2</sup> C.  
 Wheldon,<sup>2,++</sup> Tz. Kokalova,<sup>2</sup> G. de Angelis,<sup>3</sup> A. Gadea,<sup>3</sup> S. Lenzi,<sup>3</sup> S.  
 Szilner,<sup>3,\*\*\*</sup> D. R. Napoli,<sup>3</sup> W. N. Catford,<sup>4</sup> D. G. Jenkins,<sup>5</sup> and G. Royer<sup>6</sup>

<sup>1</sup>*Institut Pluridisciplinaire Hubert Curien - Département de Recherches Subatomiques,  
 UMR7178, IN2P3-CNRS et Université de Strasbourg,  
 23 rue du Loess, B.P. 28, F-67037 Strasbourg Cedex 2, France*

<sup>2</sup>*Hahn-Meitner-Institut, Glienicker Str. 100, D-14109 Berlin, Germany*

<sup>3</sup>*INFN-Lab. Nationali di Legnaro and Dipartimento di Fisica, I-35020 Padova, Italy*

<sup>4</sup>*School of Physics and Chemistry, University of Surrey, Guildford, Surrey, GU2 7XH, UK*

<sup>5</sup>*Department of Physics, University of York, York, YO10 5DD, UK*

<sup>6</sup>*Subatech, IN2P3-CNRS et Université-Ecole des Mines,  
 4 rue A. Kastler, F-44307 Nantes Cedex 3, France*

(Dated: October 26, 2021)

## Abstract

Charged particle and  $\gamma$ -decays in  $^{24}\text{Mg}^*$  are investigated for excitation energies where quasimolecular resonances appear in  $^{12}\text{C}+^{12}\text{C}$  collisions. Various theoretical predictions for the occurrence of superdeformed and hyperdeformed bands associated with resonance structures with low spin are discussed within the measured  $^{24}\text{Mg}^*$  excitation energy region. The inverse kinematics reaction  $^{24}\text{Mg}+^{12}\text{C}$  is studied at  $E_{lab}(^{24}\text{Mg}) = 130$  MeV, an energy which enables the population of  $^{24}\text{Mg}$  states decaying into  $^{12}\text{C}+^{12}\text{C}$  resonant break-up states. Exclusive data were collected with the Binary Reaction Spectrometer in coincidence with EUROBALL IV installed at the VIVITRON Tandem facility at Strasbourg. Specific structures with large deformation were selectively populated in binary reactions and their associated  $\gamma$ -decays studied. Coincident events associated with inelastic and  $\alpha$ -transfer channels have been selected by choosing the excitation energy or the entry point via the two-body  $Q$ -values. The analysis of the binary reaction channels is presented with a particular emphasis on  $^{24}\text{Mg}-\gamma$ ,  $^{20}\text{Ne}-\gamma$  and  $^{16}\text{O}-\gamma$  coincidences. New information (spin and branching ratios) is deduced on high-energy states in  $^{24}\text{Mg}$  and  $^{16}\text{O}$ , respectively.

PACS numbers: 25.70.Jj, 25.70.Pq, 24.60.Dr; 25.70.+e

\* Corresponding author: christian.beck@ires.in2p3.fr

+ Present address: Department of Physics, University of Stellenbosch, Matieland, Stellenbosch 7602, South Africa

\*\* Permanent address: IPN Orsay, Orsay, France

++ Present address: School of Physics and Astronomy, University of Birmingham, Edgbaston, Birmingham B15 2TT, United Kingdom

\*\*\* Permanent address: Ruder Bošković Institute, HR-10001 Zagreb, Croatia

## I. INTRODUCTION

The observation of resonant structures in the excitation functions for various combinations of light  $\alpha$ -cluster ( $N = Z$ ) nuclei in the energy regime from the barrier up to regions with excitation energies of  $E_x = 20$ -50 MeV remains a subject of contemporary debate [1]. These resonances have been interpreted for  $^{12}\text{C}+^{12}\text{C}$  [2], the most favorable case for the observation of quasimolecular resonances [1, 2, 3, 4, 5], in terms of nuclear molecules. The question whether the well known  $^{12}\text{C}+^{12}\text{C}$  quasimolecular resonances represent true cluster states in the  $^{24}\text{Mg}$  compound system, or whether they simply reflect scattering states in the ion-ion potential is still unresolved [1, 6, 7, 8]. In many cases, these resonant structures have been associated with strongly-deformed shapes and with clustering phenomena, predicted from the cranked  $\alpha$ -cluster model [9], the Nilsson-Strutinsky approach [10, 11], Hartree-Fock calculations [12] or other mean-field calculations [13]. Of particular interest is the relationship between superdeformation (SD) and nuclear molecules, since nuclear shapes with major-to-minor axis ratios of 2:1 have the typical ellipsoidal elongation (with quadrupole deformation parameter  $\beta_2 \approx 0.6$ ) for light nuclei [11]. Furthermore, the structure of possible octupole-unstable 3:1 nuclear shapes (with  $\beta_2 \approx 0.9$ ) - hyperdeformation (HD) - for actinide nuclei has also been widely discussed [11, 14, 15, 16, 17] in terms of clustering phenomena.

Various decay branches of highly excited  $^{24}\text{Mg}^*$  resonant states from  $^{12}\text{C}+^{12}\text{C}$ , including the emission of  $\alpha$ -particles or heavier fragments, are energetically favored. However,  $\gamma$ -decays have not been observed so far, and the  $\gamma$ -ray branches are predicted to be rather small at these excitation energies. Some old experiments have been reported [18, 19], which have searched for these very small branching ratios expected to be in the range of  $10^{-4} - 10^{-5}$  of the total width [21, 22, 23]. Very recently the radiative capture reaction  $^{12}\text{C}+^{12}\text{C}$  has been investigated [20]. The rotational bands, from the knowledge of the measured spins and excitation energies, can be extended to rather low angular momenta, where finally the  $\gamma$ -decay becomes a larger part of the total decay width. The population of such states in  $\alpha$ -cluster nuclei, which lie below the threshold for fission decays and for other particle decays, is favored in binary reactions, where at a fixed incident energy the compound nucleus is formed at an excitation energy governed by the two-body reaction kinematics. These states may be coupled to intrinsic states in  $^{24}\text{Mg}^*$  populated by a break-up process (via resonances) as

shown in Refs.[24, 25, 26, 27]. The  $^{24}\text{Mg}+^{12}\text{C}$  reaction has been extensively investigated by several measurements of the  $^{12}\text{C}(^{24}\text{Mg},^{12}\text{C}^{12}\text{C})^{12}\text{C}$  break-up channel [24, 26, 27]. Resonant breakups are found to occur from specific states in  $^{24}\text{Mg}$  at excitation energies  $E_x = 20$ -40 MeV (with spins ranging from  $J = 4\hbar$  to  $14\hbar$ ), which are linked to the ground state and also have an appreciable overlap with the  $^{12}\text{C}+^{12}\text{C}$  quasimolecular configuration. Several attempts [26] were made to link the  $^{12}\text{C}+^{12}\text{C}$  barrier resonances [2] with the break-up states. The underlying reaction mechanism is now fairly well established [27] and many of the barrier resonances appear to be correlated, indicating that a common structure is involved. This correlation strongly supports the hypothesis of the link between barrier resonances [2, 4] in  $^{12}\text{C}+^{12}\text{C}$ , and secondary minima in the Compound Nucleus (CN)  $^{24}\text{Mg}$  [9, 10, 12].

Large quadrupole deformations ( $\beta_2 = 0.6$ -1.0) and  $\alpha$ -clustering in light  $N = Z$  nuclei are known to be general phenomena at low excitation energy. For high angular momenta and higher excitation energies, very elongated shapes are expected to occur in  $\alpha$ -like nuclei for  $A_{CN} = 20$ -60. These predictions come from the generalized liquid-drop model, taking into account the proximity energy and quasi-molecular shapes [28]. In fact, highly deformed shapes and SD rotational bands have been recently discovered in several such  $N = Z$  nuclei, in particular,  $^{36}\text{Ar}$  [29] and  $^{40}\text{Ca}$  [30] using  $\gamma$ -ray spectroscopy techniques. Hyperdeformed (HD) bands in  $^{36}\text{Ar}$  nucleus and its related ternary clusterizations are theoretically predicted [31]. With the exception of the cluster decay of  $^{60}\text{Zn}$  [32, 33] and  $^{56}\text{Ni}$  [34, 35, 36] recently studied using charged particle spectroscopy, no evidence for ternary breakup has yet been reported [13, 37, 38, 39, 40, 41] in light nuclei; the particle decay of  $^{36}\text{Ar}$  SD bands (and other highly excited bands) is still unexplored. The main binary reaction channels of the  $^{24}\text{Mg}+^{12}\text{C}$  reaction, for which both quasimolecular structures [4, 42, 43] and orbiting phenomena [44] have been observed, is investigated in this work by using charged particle- $\gamma$ -ray coincidence techniques.

The present paper is organized in the following way: Sec. II describes the experimental procedures and the data analysis. Sec. III presents the exclusive  $^{24}\text{Mg}+^{12}\text{C}$  data (part of the experimental results presented here in detail have already been shortly reported elsewhere [45, 46]) which are discussed in Sec. IV. We end with a summary of the main results and brief conclusions in Sec. V.

## II. EXPERIMENTAL SET-UP

The study of charged particle- $\gamma$ -ray coincidences in binary reactions in inverse kinematics is a unique tool in the search for extreme shapes related to clustering phenomena. In this paper, we investigate the  $^{24}\text{Mg}+^{12}\text{C}$  reaction with high selectivity at a bombarding energy  $E_{lab}(^{24}\text{Mg}) = 130$  MeV by using the Binary Reaction Spectrometer (BRS) [8, 47, 48] in coincidence with the EUROBALL IV (EB) [49]  $\gamma$ -ray spectrometer installed at the VIVITRON Tandem facility of Strasbourg [6, 7, 8, 45, 46]. The  $^{24}\text{Mg}$  beam was produced and accelerated by the VIVITRON, negative  $\text{MgH}^-$  ions were extracted from the ion source and then the  $\text{MgH}$  molecules were cracked at the stripping foils of the terminal accelerator. The beam intensity was kept constant at approximately 5 pA.

The targets consisted of 200  $\mu\text{g}/\text{cm}^2$  thick foils of natural  $^{12}\text{C}$ . The effects of heavy contaminants (mainly  $^{63}\text{Cu}$  and smaller traces of W isotopes) have been estimated to be negligible. The presence of oxygen in the  $^{12}\text{C}$  target was not significant (less than  $\approx 1\%$ ). The choice of the  $^{12}\text{C}(^{24}\text{Mg},^{12}\text{C})^{24}\text{Mg}^*$  reaction implies that for an incident beam energy of  $E_{lab} = 130$  MeV an excitation energy range up to  $E^* = 30$  MeV in  $^{24}\text{Mg}$  is covered [26].

The EUROBALL IV  $\gamma$ -ray spectrometer, as shown in Fig. 1, consisted of two rings of a total of 26 Clover-Ge-detectors each composed of four Ge crystals [50] located at angles around  $90^\circ$ , and 15 Cluster-Ge-detectors [51] each consisting of seven Ge crystals at backward angles. The inner BGO scintillator array was removed.

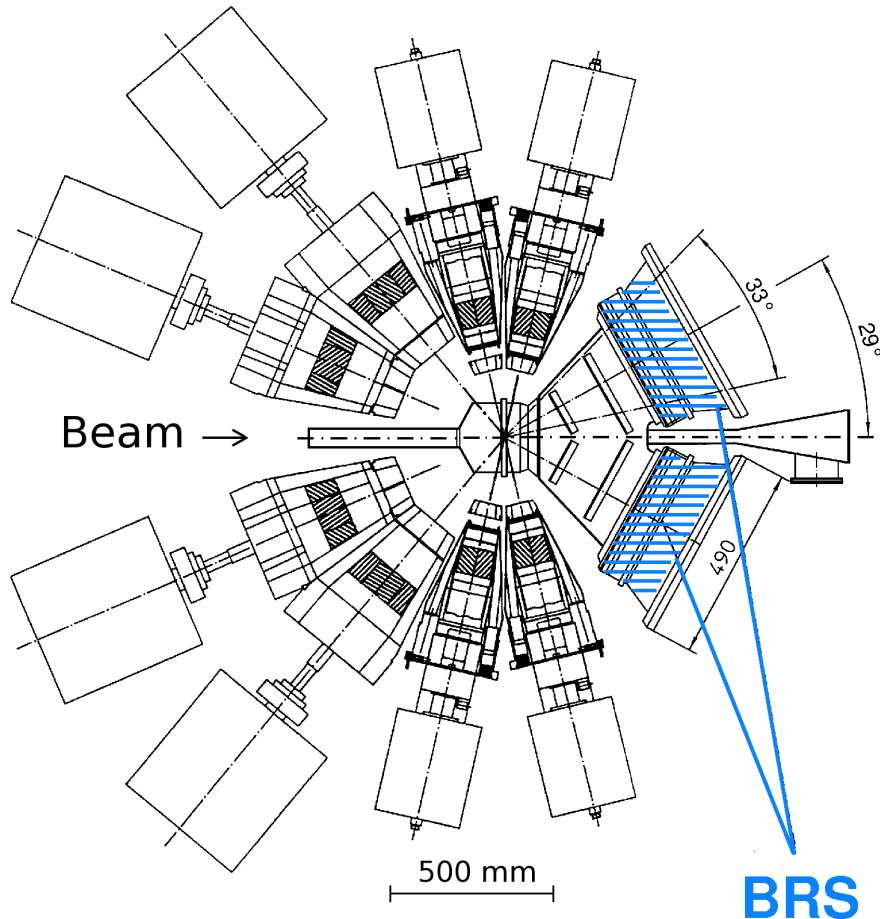
The BRS, in conjunction with EB, gives access to a novel approach for the study of nuclei at large deformations as described below.

### A. Experimental set-up of the BRS

The BRS associated with EB combines as essential elements two large-area (with a solid angle of 187 msr each) heavy-ion gas-detector telescopes in a kinematical coincidence setup at forward angles. A schematic lay-out of the actual experimental set-up of the BRS with EB is shown in Fig. 1.

A photograph of one of the two BRS telescopes is shown in Fig. 2 (top) along with a two-dimensional spectrum (bottom) obtained with a mask during a  $^{32}\text{S}+^{197}\text{Au}$  calibration run at 163.5 MeV [36]. The BRS positions were calibrated using the elastic scattering data

FIG. 1: (Color online) Schematic drawing of the scattering chamber showing the BRS arrangement for fragment detection and the  $\gamma$ -ray detectors of EB. At forward angles the two BRS gas detector telescopes are depicted, as well as two rings of Clover-Ge-detectors at angles around  $\theta = 90^\circ$  and Cluster-Ge-detectors at backward angles, respectively.

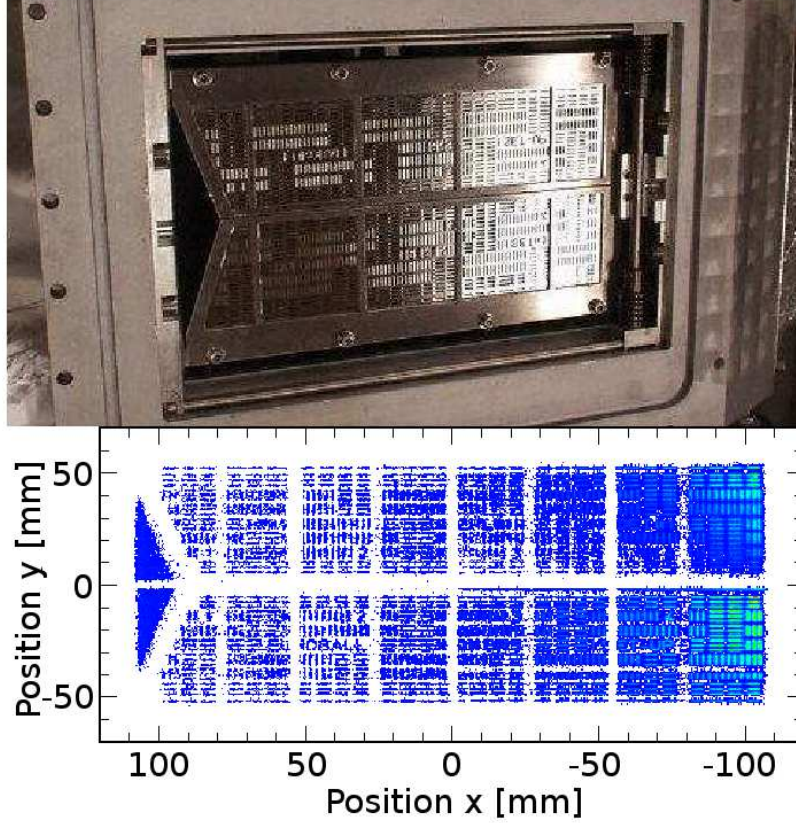


along with the known positions of slits in the movable mask in front of the BRS telescope 1.

The two BRS telescope arms are mounted symmetrically on either side of the beam axis, each covering the forward scattering angle range  $\Delta\theta = 12.5^\circ\text{-}45.5^\circ$ , i.e.  $\theta = 29^\circ \pm 16.5^\circ$ . For this reason the 30 tapered Clover-Ge-detectors of EB were removed.

Each BRS gas-detector telescope comprises two consecutive gas volumes containing a two-dimensional position sensitive low-pressure multi-wire chamber (MWC) and a Bragg-curve ionization chamber (BIC), respectively. All detection planes are four-fold segmented in order to improve the resolution and to increase the counting rate capability ( $10^5$  events/s).

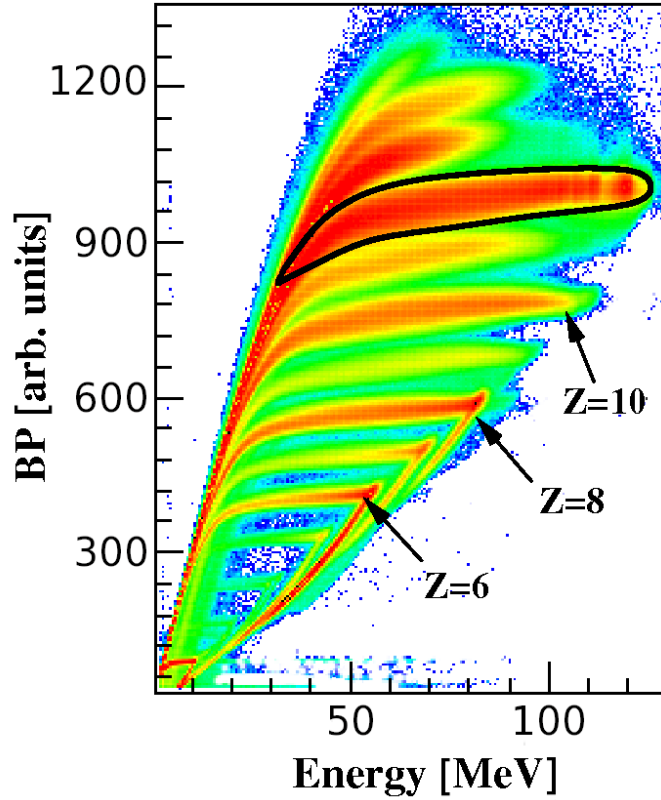
FIG. 2: (Color online) Photograph (top) showing the two sides of the mask in place, in front of one arm of the BRS telescope. The corresponding calibrated two-dimensional position  $x$  versus  $y$  (in mm) spectrum (bottom) has been registered using a  $210 \mu\text{g}/\text{cm}^2$   $^{197}\text{Au}$  target with the  $163.5 \text{ MeV } ^{32}\text{S}$  beam.



The position and time resolutions have been determined to be intrinsically  $\approx 0.5 \text{ mm}$  and  $\approx 200 \text{ ps}$ , respectively [47, 48]. In the MWCs, the in-plane and out-of-plane scattering angles  $\Theta$  and  $\Phi$ , respectively, are derived from the position ( $x$  and  $y$ ) measurements. As already shown in previous studies [40, 41], the in-plane angular correlations of two fragments need coincidence measurements for binary fission yields to be measured adequately. Unfortunately, the MWC of BRS telescope 2 could not provide us with a well functioning  $y$ -position signal (i.e.  $\Phi_2$ ), which is an essential information to check kinematical conditions of the out-of-plane correlations of ternary fission fragments. In the BICs the Bragg-Peak height (BP), Range (R), and kinetic energy (E) are measured. Two-body  $Q$ -value spectra have been reconstructed using events for which both fragments are in well selected states. The



FIG. 3: (Color online) Two dimensional BP versus E spectrum, using fragment-fragment coincidences, measured in the  $^{24}\text{Mg}(130\text{ MeV})+^{12}\text{C}$  reaction with the BRS. For Z-identification, the Z=12 gate is highlighted to show how the  $^{24}\text{Mg}$  events have been selected for the  $\gamma$ -ray spectrum displayed in Fig. 5. The three arrows indicate unambiguously the C, O and Ne fragments. Their corresponding end-point/punch-through energies, discussed in the text, can be clearly seen.



reaction mechanism - projectile breakup or ternary fission - responsible for the population of particular states could be determined from two-body kinematics. The two heavy fragments are registered using a kinematic coincidence method and identified by their charges  $Z$ . The excellent elemental identification ( $Z$ ) is illustrated by two-dimensional plots showing BP versus E. Fig. 3 displays a typical example of a two-dimensional BP vs E spectrum obtained for the  $^{24}\text{Mg}+^{12}\text{C}$  reaction. Energy calibrations were done using the energy loss program SRIM-2003 [52] (taking into account the window foils and gases) to calculate the end-point energies (punch-through) observed in the BP vs E plots. Energy spectra are given in Figs. 3 and 4 with absolute energy scales. The spectrum of Fig. 3 shows the excellent  $Z$  discrimination (the fragments with  $Z = 6, 8$  and  $10$  are indicated with respective arrows)

achieved with the BICs. It can be observed that, due to  $Q$ -value effects, the  $\alpha$ -like  $^{12}\text{C}$ ,  $^{16}\text{O}$ ,  $^{20}\text{Ne}$ ,  $^{24}\text{Mg}$  and  $^{28}\text{Si}$  nuclei are preferentially populated compared to the odd  $Z$  nuclei. This strong odd-even effect is a characteristic behavior of structure phenomena in  $^{12}\text{C}+^{24}\text{Mg}$  orbiting [44] that may still survive at  $E_{lab} = 130$  MeV. The gas pressure has been optimized to stop ions with  $Z$  larger than 9 (ejectiles with lower  $Z$ 's are not stopped in the BICs as shown by their characteristic end point/punch-through in Fig. 3).

The  $Z=12$  gate of Fig. 3 has been used to select the  $\gamma$ -ray spectrum measured in coincidence with  $^{24}\text{Mg}$  nucleus (see Fig. 5). Other well-defined  $Z$  gates can be used for the processing of the  $\gamma$ -ray spectra in coincidence with the  $^{12}\text{C}$ ,  $^{16}\text{O}$ ,  $^{20}\text{Ne}$  and  $^{28}\text{Si}$  nuclei of interest. Although mass identification has not been available in this experiment - i.e. the performance of the VIVITRON pulsing system was not better than 2ns (FWHM) -, the good energy resolution along with  $Z$ -identification allowed the different reaction mechanisms to be clearly discriminated.

Fig. 4 illustrates a typical example of a two-dimensional angle versus energy spectrum for the  $^{16}\text{O}+^{20}\text{Ne}$  exit-channel. The six regions (a-f) labelled [I] to [VI] have been defined as a function of the inelasticity of the reaction channel from the ground-state  $Q$ -value  $E^* = 0$  to full damping with  $E^*$  larger than 15 MeV. This  $\alpha$ -transfer channel will be discussed in Sec. III.B. It should be noticed that the two lines around  $21^\circ$  and  $29^\circ$  correspond to shadows produced by the supports to Mylar entrance windows of the MWC of the BRS telescope 1. The dashed line corresponds to the high-energy cutoff due to the geometrical bias of the kinematical coincidences. More details of the detectors and the experimental set-up of the BRS are given in Refs. [8, 45, 46, 47, 48].

## B. Experimental set-up of EUROBALL IV

The excellent channel selection capability of binary and/or ternary fragments (see for instance the two-dimensional angle versus energy spectrum plotted in Fig. 4 for the  $\alpha$ -transfer channel) allows clear discrimination between the reaction channels, so that EB [49] is used mostly with one- or two-fold multiplicities, for which the total  $\gamma$ -ray efficiency is very high. The removal of the conventional 30 tapered Clover-Ge-detectors of EB from the forward angles had only a very small impact on reducing the overall EB efficiency (less than 13% of the total  $\gamma$ -ray efficiency). Although no specific measurements were done during two

FIG. 4: (Color online) Two-dimensional angle versus energy spectrum, using fragment-fragment coincidences, measured for the  $^{16}\text{O}+^{20}\text{Ne}$  exit-channel. The relative intensity is shown on the side bar. The dashed red line corresponds to the high-energy cutoff due to the geometrical bias of the kinematical coincidences. The regions labelled (a) to (f) are defined in detail in the text. They correspond to the following excitation energies ranges  $E^* = 0-3$  MeV (a),  $3-6$  MeV (b),  $6-10$  MeV (c),  $10-14$  MeV (d), and  $14-19$  MeV (e), and finally region [VI] is defined for  $E^*$  larger than  $19$  MeV (f).

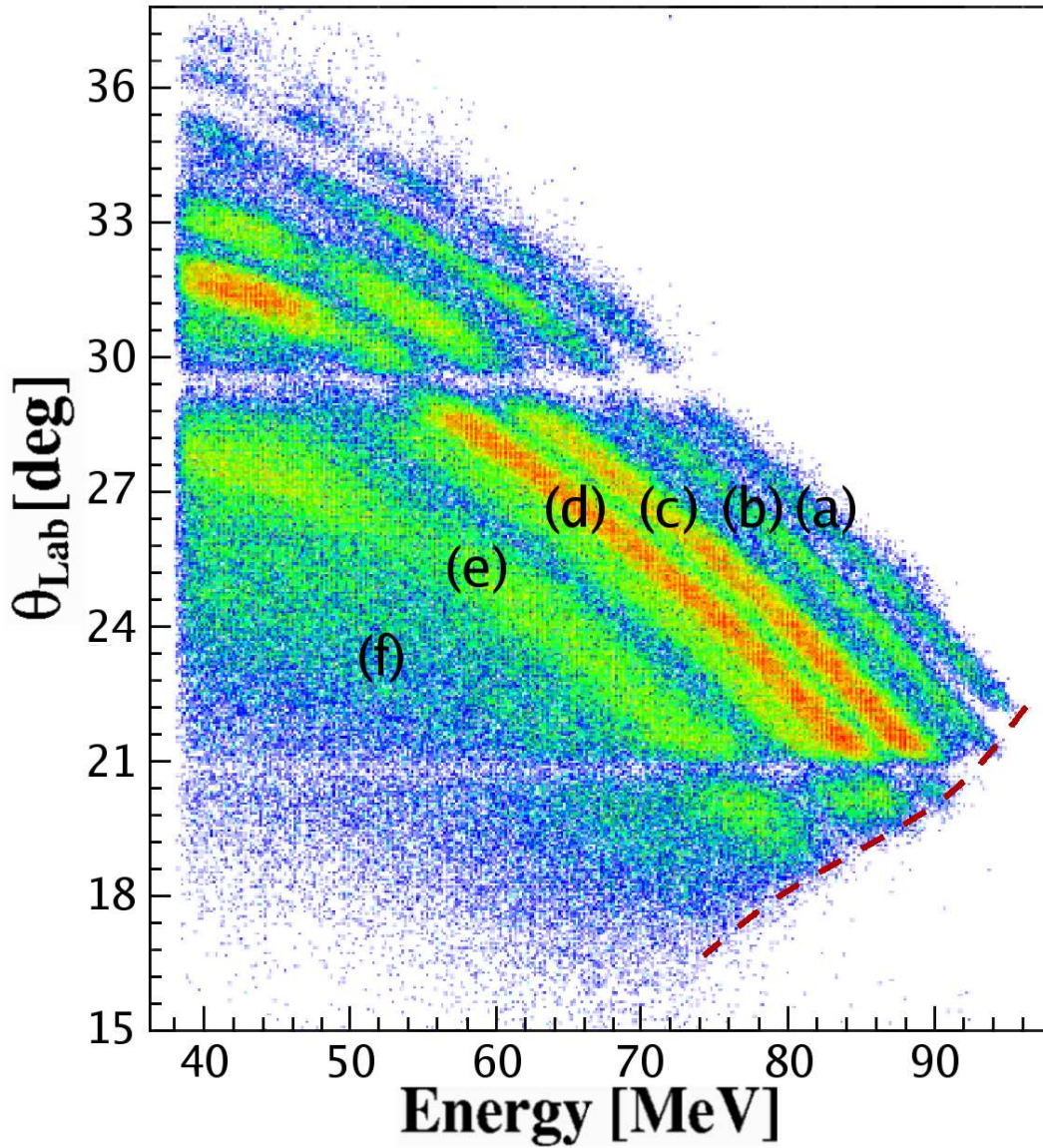
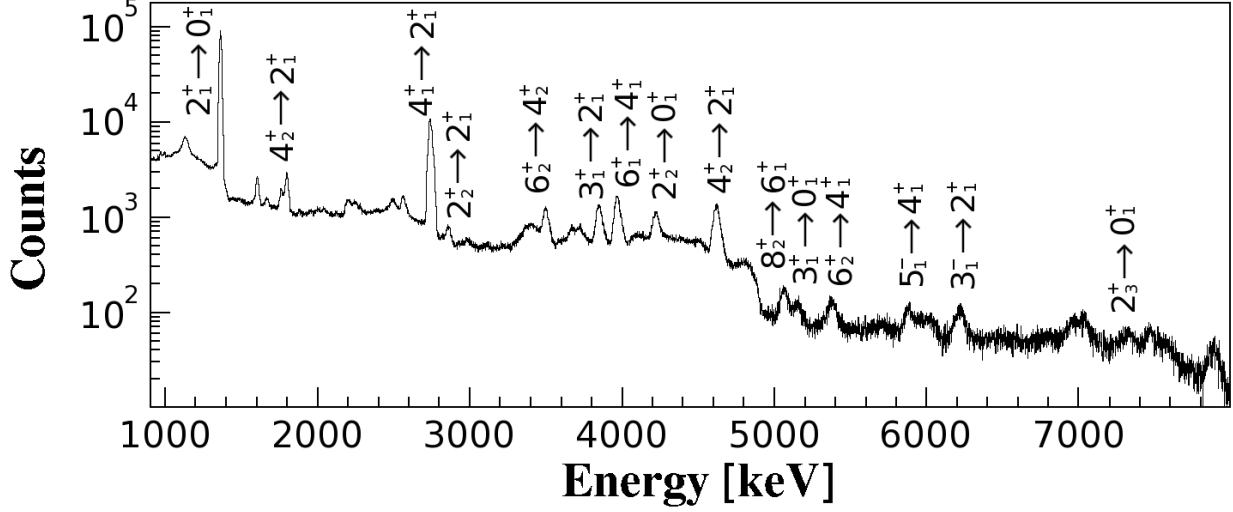


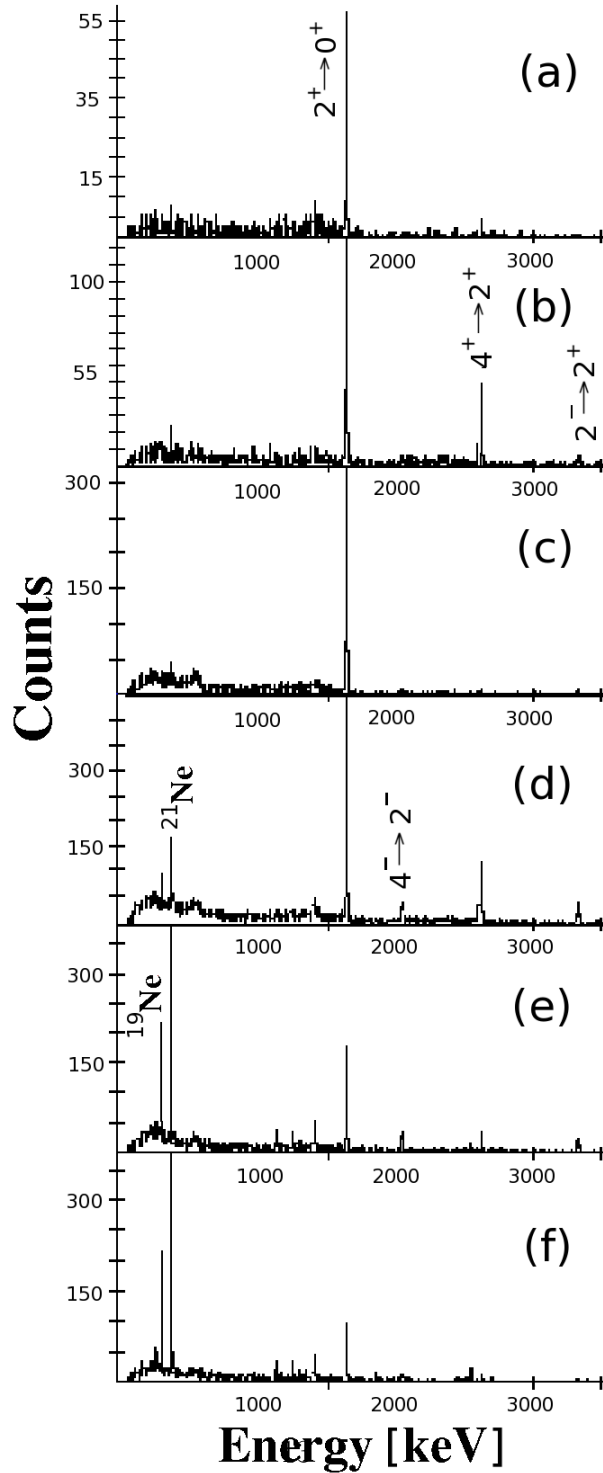
FIG. 5: Doppler corrected  $\gamma$ -ray spectrum for  $^{24}\text{Mg}$ , using fragment- $\gamma$  coincidences, measured with the BRS/EB detection system of Fig. 1. The  $^{24}\text{Mg}$  nuclei were selected with the  $Z=12$  gate marked in Fig. 3. The full details of the identified  $\gamma$ -ray transitions are given in Table I.



BRS campaigns, the absolute total  $\gamma$ -ray efficiency has been estimated to be approximately 8.5% for the present EB experiment.

In binary exit-channels, the exclusive detection of both ejectiles allows precise  $Q$ -value determination and  $Z$ -resolution, as shown in Figs. 5 and 6 for  $^{24}\text{Mg}+^{12}\text{C}$  inelastic scattering channel, and the  $^{16}\text{O}+^{20}\text{Ne}$   $\alpha$ -transfer channel, respectively. The  $\gamma$  rays were Doppler-shift corrected for the velocity of the identified outgoing binary fragments. The Doppler-shift corrections yield an energy resolution better than 40-59 keV (FWHM) for 3-4 MeV  $\gamma$  rays ( $\approx 1.3\%$  in average). The  $\gamma$ -ray spectra of Figs. 5 and 6 will be discussed in detail in the next section.

FIG. 6: Gated  $\gamma$ -ray spectra, using fragment-fragment- $\gamma$ -ray coincidences, measured for the  $^{16}\text{O}+^{20}\text{Ne}$  exit-channel. Doppler-shift corrections were applied for the velocity of the detected  $^{20}\text{Ne}$ . The six excitation energy gates labelled (a) to (f) in Fig. 4 (corresponding to excitation energies ranges  $E^* \approx 0\text{-}3$  MeV (a),  $3\text{-}6$  MeV (b),  $6\text{-}10$  MeV (c),  $10\text{-}14$  MeV (d), and  $14\text{-}19$  MeV (e), and finally the last gate (f) is applied for  $E^*$  larger than  $19$  MeV) have been used as triggers to the six  $\gamma$ -ray spectra. The main  $\gamma$ -ray transitions in  $^{20}\text{Ne}$  are labelled.



### III. EXPERIMENTAL RESULTS

The inverse kinematics of the  $^{24}\text{Mg}+^{12}\text{C}$  reaction and the negative  $Q$ -values give ideal conditions for triggering on the BRS, because the angular range is optimum for  $\theta_{lab} = 12^\circ$ - $40^\circ$  in the lab-system (with the range of  $\theta_{lab} = 12^\circ$ - $25^\circ$  for the recoils), and because the solid angle transformation favors the detection efficiency of the heavy fragments. Thus we have been able to cover a large part of the angular distribution of the binary process with good efficiency. In binary exit-channels, the exclusive detection of both ejectiles with precise  $Z$  discrimination allows excellent Doppler-shift corrections.

#### A. $^{24}\text{Mg}+^{12}\text{C}$ exit channel

Fig. 5 shows the Doppler-shift corrected  $\gamma$ -ray spectrum for  $^{24}\text{Mg}$  events in coincidence with the  $Z=12$  gate, defined in the BP vs E spectrum of Fig. 3. Most of the known transitions of  $^{24}\text{Mg}$  [53, 54, 55, 56, 57, 58, 59] can be identified in the energy range depicted in the figure and their properties are given in Table I. Weaker transitions in  $^{23}\text{Mg}$  and  $^{25}\text{Mg}$  (not marked in Fig. 5), also selected by the  $Z=12$  gate, correspond to one-neutron transfer processes. The excitation of the  $2^+$ , 1808.7 keV state of  $^{26}\text{Mg}$  arises either from a 2-neutron-transfer process or from a fusion-evaporation mechanism. These transitions are not reported in Table I. However, we note, in particular, a doublet visible in Fig. 5 near 1600 KeV which is due to the  $^{25}\text{Mg}$   $7/2^+ \rightarrow 3/2^+$  and  $^{23}\text{Mg}$   $7/2^+ \rightarrow 5/2^+$  transitions. The broad bump at 3.40 MeV corresponds to the  $9/2^+ \rightarrow 5/2^+$   $\gamma$ -ray transition.

The two most prominent  $^{24}\text{Mg}$  lines correspond, as expected, to the  $^{24}\text{Mg}$  transitions  $2_1^+ \rightarrow 0_1^+$  with  $E_\gamma = 1369$  keV (100% relative intensity) and  $4_1^+ \rightarrow 2_1^+$  with  $E_\gamma = 2754$  keV (39%), where  $0_1^+$ ,  $2_1^+$  and  $4_1^+$  are the first members of the  $^{24}\text{Mg}$   $K^\pi = 0^+$  ground state band. At higher energies, weaker lines (with relative intensities of 5-10%) are observed, corresponding to transitions with  $E_\gamma = 3990$  keV ( $6_1^+ \rightarrow 4_1^+$ ), 3866 keV ( $3_1^+ \rightarrow 2_1^+$ ), 4238 keV ( $2_2^+ \rightarrow 0_1^+$ ) and 4641 keV ( $4_2^+ \rightarrow 2_1^+$ ). The  $6_1^+$  level belongs to the ground state band and the  $2_2^+$ ,  $3_1^+$  and  $4_2^+$  to the  $^{24}\text{Mg}$   $K^\pi = 2^+$  band. As expected we see decays feeding the yrast line of  $^{24}\text{Mg}$  up to the  $8_2^+$  level at 13.21 MeV (as much as 3%). The relative intensities of the  $\gamma$ -ray transitions given in the last column of Table I are normalized to the  $2_1^+ \rightarrow 0_1^+$  1368.6 keV transition. The  $\gamma$ -ray spectrum shows mainly strong  $\gamma$ -ray transitions between positive-parity states,

however rather intense transitions are also observed from negative-parity levels ( $3_1^-$  and  $5_1^-$ ). The 1683 keV ( $4_1^- \rightarrow 3_1^-$ ) transition is weaker, with a relative intensity of much less than 1%. The deformation properties of the  $^{24}\text{Mg}$  nucleus are further discussed in Sec. IV.A.

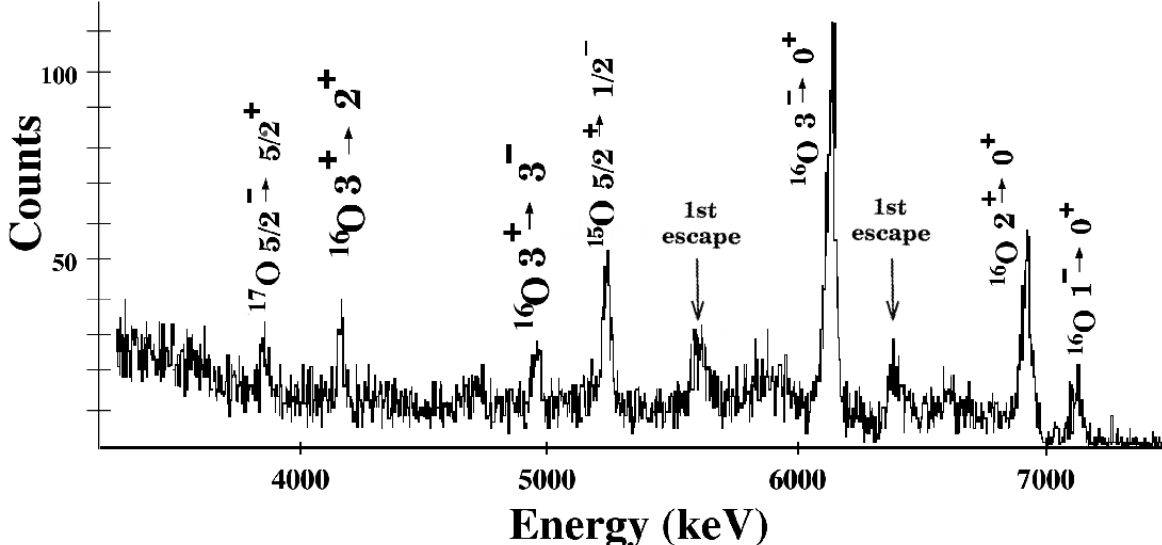
### B. $^{20}\text{Ne}+^{16}\text{O}$ exit channel

Figs. 6 and 7 display the Doppler-shift corrected  $\gamma$ -ray spectra for events in coincidence with two  $Z=8$  and  $Z=10$  gates (as the one shown for  $Z=12$  in the BP vs E spectrum of Fig. 3) defined in both arms of the BRS. Most of the known transitions of both  $^{16}\text{O}$  and  $^{20}\text{Ne}$  can be identified in the energy range depicted. The six different excitation energy gates displayed in Fig. 4 are used to generate the  $\gamma$ -ray spectra shown in Fig. 6 (low-energy transitions) and discussed in Sec. IV.B. The  $\gamma$ -ray spectrum (high-energy transitions) of Fig. 7 was triggered with the use of the gate labelled (d) for  $E^* \geq 6.5$  MeV.

Identifications of the most intense  $\gamma$  rays in  $^{20}\text{Ne}$  is straightforward and their labelling are given in Fig. 6. As expected for  $\alpha$ -transfer processes involving mutual excitations of the binary fragments, we observe decays feeding of the yrast line of the  $^{20}\text{Ne}$  nucleus. Two previously unobserved transitions in  $^{16}\text{O}$  from the decay of the  $3^+$  state at 11.08 MeV, clearly visible in the  $\gamma$ -ray spectrum of Fig. 7, have been identified for the first time (see Fig. 8 for new partial level scheme). We note that, thanks to the excellent resolving power of the EB+BRS set-up, the respective first escape peaks positions (as indicated by the two arrows) of the 6.13 MeV, 6.92 MeV and 7.12 MeV  $\gamma$ -ray transitions in  $^{16}\text{O}$  are also apparent in this spectrum.

The next step in the analysis is the use of the BRS trigger in order to select the excitation energy range by the two-body  $Q$ -value (in the  $^{16}\text{O}+^{20}\text{Ne}$  channel), and thus allowing us to study the region at rather low excitation energies (below and around particle thresholds), where  $\gamma$  decay becomes observable. The two-dimensional angle versus energy spectrum, shown in Fig. 4 for the  $\alpha$ -transfer channel, allow us to select well defined excitation energy ( $Q$ -value) regions. We define six different energy regions ranging from the (g.s.) elastic and inelastic ( $^{20}\text{Ne}$ ,  $2_1^+$ ) transfer (defined as gate (a)) up to highly excited states (namely the deep-inelastic gates (e) and (f)). The other gates correspond to energy regions where mutual inelastic excitation processes are dominant. The oscillations observed at large angles in the ‘‘gate [I]’’ region correspond - as for the  $^{24}\text{Mg}+^{12}\text{C}$  exit-channel (not shown) - to the

FIG. 7:  $^{16}\text{O}$  high-energy  $\gamma$ -ray spectrum produced by the  $^{16}\text{O}+^{20}\text{Ne}$  exit-channel with the gate (d) of Fig. 4 (for  $E^* = 10\text{-}14$  MeV as defined in the text). Doppler-shift corrections have been applied for O fragments detected in the BRS. The two arrows show the respective first escape peaks positions of the 6.13 MeV and 6.92 MeV  $\gamma$ -ray transitions in  $^{16}\text{O}$ .



oscillatory nature of the angular distribution of the  $\alpha$  transfer, and indicate the dominance of the grazing partial waves already observed for the  $^{24}\text{Mg}+^{12}\text{C}$  reaction [1, 4, 42, 43]. The second (gate (b)) and third (gate (c))  $E^*$  regions include mainly the second excited state of  $^{20}\text{Ne}$  ( $4_1^+$ , 4248 keV). The following region (gate (d)) with the largest intensity arises from the corresponding mutual excitations with the excitation of the ( $3^-$ , 6129 keV) collective state of  $^{16}\text{O}$ . The last two gates correspond to more and more energy damped collisions (deep-inelastic, orbiting [44] and fusion-fission [41]) with non-oscillatory angular distributions.

We have also analysed the  $^{12}\text{C}+^{12}\text{C}$  coincidences to investigate  $^{12}\text{C}-^{12}\text{C}-^{12}\text{C}$  ternary decays of  $^{36}\text{Ar}$ . Unfortunately, an accurate out-of-plane correlation could not be measured. Therefore, the hypothesis of  $^{36}\text{Ar}$  hyperdeformed shapes, predicted by preliminary calculations performed in the framework of the generalized liquid-drop model [28], will need further experimental investigations with higher selectivity.



## IV. DISCUSSION

### A. Deformation properties of the $^{24}\text{Mg}$ nucleus

The fact that Fig. 5 shows almost exclusively  $^{24}\text{Mg}$   $\gamma$ -ray transitions between positive-parity states, with weaker transitions observed from negative-parity levels (as indicated by Table I) has been explained by the specific nature of  $^{24}\text{Mg}$  [56] which, in its ground state, has a prolate shape. The  $^{24}\text{Mg}$  nucleus appears to be populated primarily through its first two rotational bands,  $K^\pi = 0^+$ , ( $2_1^+$  (1369 keV),  $4_1^+$  (4123 KeV),  $6_1^+$  (8113 keV)) and  $K^\pi = 2^+$  ( $2_2^+$  (4236 keV),  $3_1^+$  (5235 keV),  $4_2^+$  (6010 keV),  $6_2^+$  (9528 keV)), which are associated with stable prolate deformations, according to standard shell-model calculations [60]. In a prior measurement at a lower bombarding energy, a selective population of natural-parity states has been found to be favored in the  $^{24}\text{Mg}+^{12}\text{C}$  orbiting reaction [44], with a suppression of the  $3_1^+$  (5235 keV) and  $5_1^+$  (7812 keV) states of the  $K = 2$  band of  $^{24}\text{Mg}$ . In the present data, the  $3^+$  state is strongly populated, whereas the  $5^+$  state is moderately populated in sharp contrast with the previous experiment [44]. Decays from even higher-energy  $6_1^+$  (8113 keV) and  $6_2^+$  (9528 keV) levels from the  $K^\pi = 0^+$  and  $K^\pi = 2^+$  bands, respectively, are also clearly visible in the spectrum. The selectivity of natural parity states in the  $^{24}\text{Mg}+^{12}\text{C}$  exit-channel indicated that the orbiting processes, found to have strong yields at 3-4 times the Coulomb barrier [44], are competitive. The rather strong populations of the  $3^+$  and  $5^+$  states at  $E_{lab} = 130$  MeV suggest that the orbiting process has a smaller contribution than at lower incident energies. This would be in conflict with the survival of orbiting-like yields recently measured in the  $^{20}\text{Ne}+^{12}\text{C}$  reaction up to  $E_{lab} = 200$  MeV [61, 62].

Although there is an indication of an unknown  $\gamma$  ray around 5.95 MeV we cannot confirm its interpretation as to be the earlier reported  $10_1^+ \rightarrow 8_2^+$  5927 keV transition [57].

The strong population of a broad peak (most probably due to a number of different states) around  $E_x = 10$  MeV and states in the non-yrast  $K = 2$  rotational band was observed in the  $^{12}\text{C}(^{12}\text{C},\gamma)$  radiative capture reaction [20, 58] at two resonant energies ( $E_{c.m.} = 6.0$  and 6.8 MeV). On the other hand the population of the observed states which are members of the  $K = 2$ , does appear to be selectively enhanced in the present experiment.

It has been shown using the  $\gamma$ - $\gamma$  coincidences that most of the states of Fig. 5 belong to cascades which contain the characteristic 1369 keV  $\gamma$ -ray and pass through the lowest  $2^+$

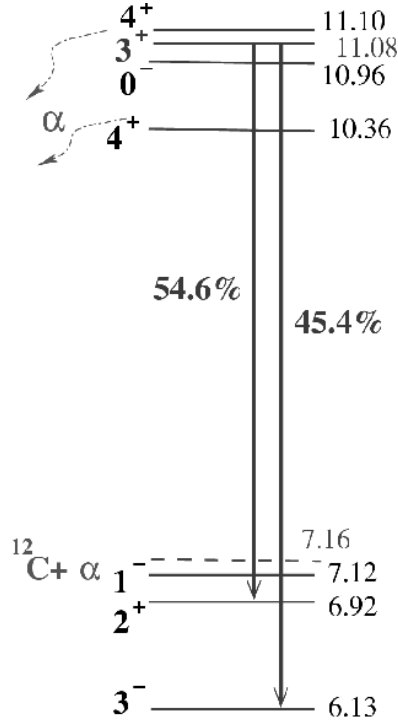
state in  $^{24}\text{Mg}$ . Still, a number of transitions in the high-energy part of the spectrum (6 MeV - 9 MeV) have not been clearly identified. The reason why the search for a direct  $\gamma$  decay in  $^{12}\text{C}+^{12}\text{C}$  has not been conclusive so far [18, 19] is due to the excitation energy in  $^{24}\text{Mg}$  as well as the spin region ( $8\hbar$  -  $12\hbar$ ) which were probably chosen too high, as in radiative capture experiments [20, 58], for instance. As the situation about  $^{12}\text{C}+^{12}\text{C}$  quasimolecular resonances is rather complex, future experimental works will have to investigate 10 MeV transitions involving low spin (0 or  $2\hbar$ ) states. In the case of the break-up reaction, the  $4\hbar$  -  $6\hbar$  spin region has been reached, however because of poor statistics none of the unplaced transitions can be assigned to the intra-band  $E_2$   $\gamma$ -ray expected to be enhanced between resonant molecular states [21, 22, 23].

Although charged-particle decays are strongly competitive at high excitation energy, high-energy  $\gamma$ -ray transitions in  $^{24}\text{Mg}$  have been found (but with no clear assignment). However, the analysis of the  $^{24}\text{Mg}+^{12}\text{C}$  exit-channel appears inconclusive as far as the search for the intra-band  $\gamma$ -rays is concerned. One should keep in mind that the de-excitation spectra can be very different from the excitation ones. Some degrees of freedom can have a major role in the excitation mechanism (in matrix elements) whereas they can play a minor one in the de-excitation processes, as the de-excitation process may, in fact, be dominated by very small components in the wave function. Even if they are strongly excited by some open channels (excitation), they can play a very small role in the actual  $\gamma$ -ray spectra we see (de-excitation). Since this intra-band  $\gamma$  ray lies so far from the  $^{24}\text{Mg}$  yrast line it is much more difficult to identify this band experimentally than it was for the analogous SD bands in heavier nuclei such as  $^{36}\text{Ar}$  [29] and  $^{40}\text{Ca}$  [30], for instance. In addition, the actual branching ratios may be smaller than the calculations using the  $\alpha$ -cluster model [23].

### B. Gamma-ray spectroscopy of the $^{20}\text{Ne}$ and $^{16}\text{O}$ nuclei

The first two gates of Fig. 4 with excitation energies of  $0 \leq E^* \leq 3$  MeV and  $3 \leq E^* \leq 6$  MeV, respectively, allow essentially the feeding of the first two excited states of the  $^{20}\text{Ne}$  yrast g.s. band to be observed, i.e. the  $\gamma$  rays from  $2^+ \rightarrow 0^+$  and from  $4^+ \rightarrow 2^+$  are dominant in Fig. 6. When  $E^*$  is increased by choosing the two  $E^*$  gates:  $10 \leq E^* \leq 14$  MeV and  $E^* \geq 14$  MeV, higher-energy states are observed in  $^{20}\text{Ne}$ . Other  $\gamma$  rays from  $^{21}\text{Ne}$  and  $^{19}\text{Ne}$  nuclei appear with increasing yields. They correspond respectively to the  $2p1n$  multi-

FIG. 8: New partial (high-energy) level scheme of  $^{16}\text{O}$  corresponding to  $\gamma$ -ray transitions observed in Fig. 7.



nucleon transfer channel (or  $\alpha$  transfer followed by a subsequent neutron evaporation) and  $\alpha n$  transfer channel, respectively. The  $5/2^+ \rightarrow 1/2^-$  transition of  $^{15}\text{O}$  corresponds also to a multi-nucleon transfer (i.e.  $2p1n$ ) process. It is also worth noting that feeding of the  $^{20}\text{Ne}$  states appears to saturate with increasing  $E^*$ , since binary decays decrease compared to sequential three-body decay channels such as  $^{16}\text{O} + ^{20}\text{Ne}^* \rightarrow ^{16}\text{O} + ^{16}\text{O} + \alpha$ . This saturation effect is known to occur for orbiting processes due to an angular momentum limitation as evidenced, for example, in  $^{28}\text{Si} + ^{12}\text{C}$  deep-inelastic collisions [63].

With appropriate Doppler-shift corrections applied to Oxygen fragments identified in the BRS, it has been possible to extend the knowledge of the level scheme of  $^{16}\text{O}$  at high energies [54, 55, 64], well above the  $^{12}\text{C} + \alpha$  threshold (7.162 MeV), which is given in Fig. 8 (dashed line) for the sake of comparison.

New information has been deduced on branching ratios of the decay of the  $3^+$  state of  $^{16}\text{O}$  at  $11.085 \text{ MeV} \pm 3 \text{ keV}$ . This state does not  $\alpha$ -decay because of non-natural parity [64], in contrast to the two neighbouring  $4^+$  states (at 10.36 MeV and 11.10 MeV, respectively as indicated in Fig. 8) to the  $2^+$  state at 6.92 MeV ( $54.6 \pm 2 \%$ ). By considering all the four

possibilities of transitions types of the  $3^+$  state (i.e.  $E_1$  and  $M_2$  for the  $3^+ \rightarrow 3^-$  transition and,  $M_1$  and  $E_2$  for the  $3^+ \rightarrow 2^+$  transition), our calculations yield to the conclusion that a value for the decay width  $\Gamma_\gamma$  is fifty times lower than the one given in the literature [54, 55], it means  $\Gamma_{3^+} < 0.23$  eV. This result is important as it is the last known  $\gamma$ -decay level for the well studied  $^{16}\text{O}$  nucleus [54, 55]. Much more details on the gamma-decay width estimates can be found elsewhere [65, 66].

There is a renew interest in the spectroscopy of the  $^{16}\text{O}$  nucleus at high excitation energy (i.e. larger than 12 MeV) as shown in Ref. [67], for instance. Charged particle data [68, 69] have been recently re-analysed to study higher excitation energy  $4\alpha$  states of the  $^{16}\text{O}$  nucleus near the  $^8\text{Be}+^8\text{Be}$  (14.619 MeV) and  $^{12}\text{C}+\alpha$  (14.611 MeV) decay thresholds. In the framework of the study of Bose-Einstein Condensation (BEC)  $\alpha$ -particle state in light  $N=Z$  nuclei, the experimental signature of BEC in  $^{16}\text{O}$  is at present of the highest priority. An equivalent  $\alpha$ +”Hoyle” state in  $^{12}\text{C}$  is predicted to be the  $0_6^+$  state of  $^{16}\text{O}$  at about 15.1 MeV, which energy is just lying (i.e.  $\approx 700$  keV) above the  $4\alpha$ -particle breakup threshold [70]. However, any state in  $^{16}\text{O}$  equivalent to the so-called ”Hoyle” state in  $^{12}\text{C}$  is most certainly going to decay by particle emission, with very small, probably un-measurable  $\gamma$ -decay branches. Very efficient particle-detection techniques will have to be used in the near future as such BEC states will be expected to decay by alpha emission to the ”Hoyle” state, and could be associated with resonances in  $\alpha$ -particle inelastic scattering on  $^{12}\text{C}$  leading to that state, or be observed in  $\alpha$ -particle transfer to the  $^8\text{Be}-^8\text{Be}$  final state as observed by P. Chevallier and coworkers back in the sixties [71]. Another possibility might be to perform Coulomb excitation measurements with intense  $^{16}\text{O}$  beams at intermediate energies.

## V. CONCLUSION

The connection of  $\alpha$ -clustering, quasimolecular resonances, orbiting phenomena and extreme deformations (SD, HD, ...) has been discussed in this work by using  $\gamma$ -ray spectroscopy of coincident binary fragments from either inelastic excitations and direct transfers (with small energy damping and spin transfer) or from orbiting (fully damped) processes [41]. Exclusive data were collected with the Binary Reaction Spetrometer (BRS) in coincidence with EUROBALL IV installed formerly at the VIVITRON Tandem facility of Strasbourg. The search for the  $\gamma$ -ray decay of a  $^{12}\text{C}+^{12}\text{C}$  molecule [1, 2] as populated by projectile breakup has been undertaken. The existence of intense high-energy  $\gamma$ -rays in the  $E_x = 10$  MeV region in  $^{24}\text{Mg}^*$  strongly populated in the  $^{24}\text{Mg}+^{12}\text{C}$  reaction is found to be of great interest. Most of these  $\gamma$ -rays may correspond to the doorway low-spin states recently observed in the radiative capture reaction  $^{12}\text{C}(^{12}\text{C},\gamma)^{24}\text{Mg}^*$  [20, 58].

The striking selectivity of natural parity states in the  $^{24}\text{Mg}+^{12}\text{C}$  exit-channel indicates that the orbiting processes dominant in the vicinity of the Coulomb barrier [44] still survives at  $E_{lab} = 130$  MeV. From a careful analysis of the  $^{16}\text{O}+^{20}\text{Ne}$   $\alpha$ -transfer exit-channel (strongly populated by orbiting) new information has been deduced on branching ratios of the decay of the  $3^+$  state of  $^{16}\text{O}$  at 11.089 MeV. This result is encouraging for a complete  $\gamma$ -ray spectroscopy of the  $^{16}\text{O}$  nucleus at high excitation energy. Of particular interest is the quest for the corresponding  $4\alpha$  states near the  $^8\text{Be}+^8\text{Be}$  and  $^{12}\text{C}+\alpha$  decay thresholds.

The occurrence of the collinear ternary decay from hyperdeformed shapes of  $^{56}\text{Ni}$  and  $^{60}\text{Zn}$  nuclei has been also investigated for  $^{36}\text{Ar}$  in the present work, but could not be firmly confirmed. However, this hypothesis in accordance with preliminary calculations performed in the framework of the generalized liquid-drop model [28] will need further experimental investigations with higher selectivity. The search for extremely elongated configurations (HD) in rapidly rotating medium-mass nuclei, which has been pursued exclusively using  $\gamma$ -ray spectroscopy, will have to be performed in conjunction with charged particle spectroscopy in the near future (see [35, 36]).

**Acknowledgments:** We thank both the staff of the VIVITRON for providing us with good stable  $^{24}\text{Mg}$  beams and the EUROBALL group of Strasbourg for the excellent support in carrying out the experiment. Prof. Z. Dombradi and Prof. E. Uegaki are acknowledged for their careful reading of the manuscript. This work was supported by the french IN2P3/CNRS, the german ministry of research (BMBF grant under contract Nr.06-OB-900), and the EC Euroviv contract HPRI-CT-1999-00078. S.T. would like to express his gratitude for the warm hospitality during his three month stay in Strasbourg to the IReS and, he is grateful for the financial support obtained from the IN2P3, France.

- 
- [1] W. Greiner, J. Y. Park, and W. Scheid, *Nuclear Molecules*, Ed. World Scientific Publishing Co., Singapore, 1995.
- [2] K. A. Erb and D. A. Bromley, In *Treatise on Heavy Ion Science*, ed. by D.A. Bromley, Vol. **3**, Plenum, New York (1985) p. 201.
- [3] A. Morsad, F. Haas, C. Beck, and R. M. Freeman, *Z. Phys.* **A338**, 61 (1991).
- [4] C. Beck, Y. Abe, N. Aissaoui, B. Djerroud, and F. Haas, *Phys. Rev. C* **49**, 2618 (1994); *Nucl. Phys.* **A583**, 269 (1995).
- [5] S. Szilner, Z. Basrak, R. M. Freeman, F. Haas, A. Morsad, and C. Beck, *Phys. Rev. C* **55**, 1312 (1997).
- [6] C. Beck, *Int. J. Mod. Phys. E* **13**, 9 (2004); arXiv:[nucl-th/0401005](#) (2004).
- [7] C. Beck, *Nucl. Phys.* **A738**, 24 (2004); arXiv:[nucl-ex/0401004](#) (2004).
- [8] C. Beck *et al.*, *Nucl. Phys.* **A734**, 453 (2004); arXiv:[nucl-ex/0309007](#) (2003).
- [9] S. Marsh and W. D. Rae, *Phys. Lett. B* **180**, 185 (1986).
- [10] G. Leander and S. E. Larsson, *Nucl. Phys.* **A239**, 93 (1975).
- [11] A. Åberg and L.-O. Jonsson, *Z. Phys.* **349**, 205 (1994).
- [12] H. Flocard, P. H. Heenen, S. J. Krieger, and M. S. Weiss, *Prog. Theor. Phys.* **72**, 1000 (1984).
- [13] R. K. Gupta, S. K. Patra, P. D. Stevenson, C. Beck, and W. Greiner, *J. Phys. G: Nucl. Part. Phys.* **35**, 075106 (2008).
- [14] S. Cwiok, W. Nazarewicz, J. X. Saladin, W. Plociennik, and A. Johnson, *Phys. Lett. B* **322**, 304 (1994).
- [15] J. Cseh, A. Algora, J. Darai, and P. O. Hess, *Phys. Rev. C* **70**, 034311 (2004).
- [16] A. V. Andreev, G. G. Adamian, N. V. Antonenko, S. P. Ivanova, S. N. Kulin, and W. Scheid, *Eur. Phys. J. A* **30**, 579 (2006).
- [17] G. G. Adamian, N. V. Antonenko, R. V. Jolos, S. P. Ivanova, Yu. V. Palchikov, T. M. Shneidman, A. Andreev, and W. Scheid, *Int. J. Mod. Phys. E* **16**, 1021 (2007).
- [18] R. L. McGrath, D. Abriola, J. Karp, T. Renner, and S. Y. Zhu, *Phys. Rev. C* **24**, 2374 (1981).
- [19] V. Metag, A. Lazzarini, K. Lesko, and R. Vandenbosch, *Phys. Rev. C* **25**, 1486 (1982).
- [20] D. G. Jenkins *et al.*, *Phys. Rev. C* **76**, 044310 (2007).
- [21] D. Baye and P. Descouvemont, *Nucl. Phys.* **A419**, 397 (1984).

- [22] E. Uegaki, Prog. Theor. Suppl. **132**, 135 (1998).
- [23] J. Zhang, A. C. Merchant, and W. D. M. Rae, Nucl. Phys. **A613**, 14 (1997).
- [24] B. R. Fulton *et al.*, Phys. Lett. B **181**, 233 (1986); Phys. Lett. B **267**, 325 (1991).
- [25] J. Wilczynski, K. Siwek Wilczynska, Y. Chan, S. B. Gazes, and R. G. Stokstad, Phys. Lett. B **181**, 229 (1986).
- [26] N. Curtis *et al.*, Phys. Rev. C **51**, 1554 (1995); Phys. Rev. C **61**, 064606 (2000).
- [27] S. M. Singer *et al.*, Phys. Rev. C **62**, 054609 (2000).
- [28] G. Royer, K. Degiorgio, M. Dubillot, and E. Leonard, J. Phys. Conf. Ser.: **111**, 012052 (2008).
- [29] C. E. Svensson *et al.*, Phys. Rev. Lett. **85**, 2693 (2000); Phys. Rev. C **63**, 061301 (2001).
- [30] E. Ideguchi *et al.*, Phys. Rev. Lett. **87**, 222501 (2001).
- [31] A. Algora, J. Cseh, J. Darai, and P. O. Hess, Phys. Lett. B **639**, 451 (2006).
- [32] V. Zhrebchevsky, W. von Oertzen, D. Kamanin, B. Gebauer, S. Thummerer, Ch. Schulz, and G. Royer, Phys. Lett. B **646**, 12 (2007).
- [33] W. von Oertzen, V. Zhrebchevsky, B. Gebauer, Ch. Schulz, S. Thummerer, D. Kamanin, G. Royer, and Th. Wilpert, Phys. Rev. C **78**, 044615 (2008).
- [34] W. von Oertzen *et al.*, Eur. Phys. J. A **36**, 279 (2008).
- [35] W. von Oertzen *et al.*, J. Phys. Con. Ser.: **111**, 012051 (2008).
- [36] C. Wheldon *et al.*, Nucl. Phys. **A811**, 276 (2008).
- [37] N. Curtis *et al.*, Phys. Rev. C **53**, 1804 (1996).
- [38] A. St. J. Murphy *et al.*, Phys. Rev. C **53**, 1963 (1996).
- [39] C. Beck and A. Szanto de Toledo, Phys. Rev. C **53**, 1989 (1996); arXiv:[nucl-th/9512025](https://arxiv.org/abs/nucl-th/9512025) (1995).
- [40] C. Beck *et al.*, Eur. Phys. Jour. A **2**, 281 (1998); arXiv:[nucl-ex/9808004](https://arxiv.org/abs/nucl-ex/9808004) (1998).
- [41] S. J. Sanders, A. Szanto de Toledo, and C. Beck, Phys. Rep. **311**, 487 (1999); and references therein; see also arXiv:[nucl-ex/9904009](https://arxiv.org/abs/nucl-ex/9904009) (1999).
- [42] J. L. C. Ford, J. Gomez del Campo, D. Shapira, M. R. Clover, M. R. DeVries, B. R. Fulton, R. Ost, and C. F. Maguire, Phys. Lett. B **89**, 48 (1979).
- [43] J. Schimizu *et al.*, Phys. Lett. B **112**, 323 (1982).
- [44] A. Glaesner, W. Dünneweber, M. Bantel, W. Hering, D. Konnerth, R. Ritzka, W. Trautmann, W. Trombik, and W. Zipper, Nucl. Phys. **A509**, 331 (1990); and references therein.
- [45] C. Beck *et al.*, Int. Jour. Mod. Phys. E **17**; 2049 (2008).



- [46] C. Beck *et al.*, in AIP Conf. Proc. **1098**, 207 (2009); Proceedings of the Fusion08 Conference, New Aspects of Heavy Ion Collisions Near the Coulomb Barrier, September 22 - 26, 2008, Chicago, Illinois, USA; arXiv:**0811.0992** (2008).
- [47] S. Thummerer *et al.*, Physica Scripta Vol. **T88**, 114 (2000).
- [48] B. Gebauer *et al.*, *Achievements with the Euroball spectrometer*, eds. W. Korten and S. Lunardi, p. 135 (2003).
- [49] F. A. Beck, Prog. Part. Nucl. Phys. **28**, 443 (1992); J. Simpson, Z. Phys. **A358**, 139 (1997).
- [50] G. Duchêne, F. A. Beck, P. J. Twin, G. de France, D. Curien, L. Han, C. W. Beausang, M. A. Bentley, P. J. Nolan, and J. Simpson, Nucl. Instr. Meth. **A432**, 90 (1999).
- [51] J. Eberth, H. G. Thomas, P. von Brentano, R. M. Lieder, H. M. Jäger, H. Kämmerling, M. Berst, D. Gutknecht, and R. Henck, Nucl. Instr. Meth. **A369**, 135 (1996).
- [52] J. F. Ziegler, Nucl. Instr. Meth. **B219**, 1027 (2004); see also <http://www.SRIM.org>.
- [53] W. J. Vermeer, D. M. Pringle, and I. F. Wright, Nucl. Phys. **A485**, 380 (1988).
- [54] P. M. Endt, Atomic Data and Nucl. Data Tables **55**, 171 (1993).
- [55] <http://www.nndc.bnl.gov>
- [56] C. Beck *et al.*, Phys. Rev. C **63**, 014607 (2000).
- [57] I. Wiedenhöver *et al.*, Phys. Rev. Lett. **87**, 142502 (2001).
- [58] D. G. Jenkins *et al.*, Phys. Rev. C **71**, 041301(R) (2005).
- [59] M.-D. Salsac *et al.*, Nucl. Phys. A **811**, 1 (2008).
- [60] M. Carchidi and B. H. Wildenthal, Phys. Rev. C **37**, 1681 (1988).
- [61] C. Bhattacharya *et al.*, Phys. Rev. C **72**, 021601(R) (2005); arXiv:**nucl-ex/0503001** (2005).
- [62] Aparajita Dey *et al.*, Phys. Rev. C **75**, 064606 (2007); arXiv:**0704.1209**[nucl-ex] (2007).
- [63] D. Shapira, D. Schull, J. L. C. Ford, Jr., B. Shivakumar, R. L. Parks, R. A. Cecil, and S. T. Thornton, Phys. Rev. Lett. **53**, 1634 (1984).
- [64] D. A. Bromley, H. E. Gove, J. A. Kuehner, A. E. Litherland, and E. Almqvist, Phys. Rev. **114**, 758 (1959); J. A. Kuehner, A. E. Litherland, E. Almqvist, D. A. Bromley, and H. E. Gove, **114**, 775 (1959).
- [65] A. Sànchez i Zafra, Ph.D. Thesis, Université Louis Pasteur, Strasbourg (2006); Report IPHC **06-010**(unpublished).
- [66] A. Sànchez i Zafra *et al.*, in Proceedings *XLIII Intern. Winter Meeting in Nuclear Physics*, Bormio, Italy, 14-18 March 2005, Eds. I. Iori and A. Bortolotti, p.224 [Ricerca Scientifica ed

- Educazione Permanente Supp. 124, 224 (2005).]
- [67] N. J. Ashwood *et al.*, J. Phys. G: Nucl. Part. Phys. **36**, 055105 (2009).
  - [68] M. Freer *et al.*, Phys. Rev. C **51**, 1682 (1995).
  - [69] M. Freer, Int. Jour. Mod. Phys. E **17**, 2086 (2008).
  - [70] Y. Funaki, T. Yamada, H. Horiuchi, G. Ropke, P. Schuck, and A. Tohsaki, Phys. Rev. Lett. **101**, 082502 (2008).
  - [71] P. Chevallier, F. Scheibling, G. Goldring, I. Plessner, and M.W.Sachs, Phys. Rev. **160**, 827 (1967).

$E_{\gamma}^{exp}$ (keV)	$\gamma$ -ray transition	$E_{level}^*$ (keV)	$I_{\gamma}$ (%)
1368.6	$2_1^+ \rightarrow 0_1^+$	1368.6	100
1683.3	$4_1^- \rightarrow 3_1^-$	9299.8	0.32
1771.9	$4_2^+ \rightarrow 2_2^+$	6010.3	2.11
2576.9	$5_1^+ \rightarrow 3_1^+$	7812.2	2.11
2754.0	$4_1^+ \rightarrow 2_1^+$	4122.9	39.3
2869.5	$2_2^+ \rightarrow 2_1^+$	4238.4	2.98
3517.0	$6_2^+ \rightarrow 4_2^+$	9528.0	4.50
3689.0	$(4^-, 5^+) \rightarrow 4_1^+$	7812.2	1.53
3747.0	$(6^+, 7^-, 8^+) \rightarrow 6_1^+$	11860	1.47
3866.2	$3_1^+ \rightarrow 2_1^+$	5235.2	7.22
3990.0	$6_1^+ \rightarrow 4_1^+$	8113.0	6.52
4238.4	$2_2^+ \rightarrow 0_1^+$	4238.4	4.96
4641.2	$4_2^+ \rightarrow 2_1^+$	6010.3	10.2
5063.2	$0_2^+ \rightarrow 2_1^+$	6432.5	1.48
5099.0	$8_2^+ \rightarrow 6_1^+$	13213	3.17
5404.0	$6_2^+ \rightarrow 4_1^+$	9528.0	1.13
5904.2	$5_1^- \rightarrow 4_1^+$	10027.9	1.29
6246.9	$3_1^- \rightarrow 2_1^+$	7616.5	1.23
6988.3	$3_2^- \rightarrow 2_1^+$	8358.1	0.25
7069.5	$4_3^+ \rightarrow 2_1^+$	8439.3	0.24
7347.8	$2_3^+ \rightarrow 0_1^+$	7349.1	0.89
7554.0	$1_1^- \rightarrow 0_1^+$	7555.3	0.63
7615.2	$3_1^- \rightarrow 0_1^+$	7616.5	0.10
7914.3	$2_4^+ \rightarrow 2_1^+$	9284.4	0.27
8436.8	$1_2^- \rightarrow 0_1^+$	8438.4	0.039
8990.2	$2_5^+ \rightarrow 2_1^+$	10360.7	0.075
9816.5	$(1,2,3) \rightarrow 2_1^+$	11187.3	0.023

TABLE I:  $\gamma$ -ray transitions observed in coincidence (see Fig. 5) with  $^{24}\text{Mg}$  ( $Z=12$  gate marked in Fig. 3). The efficiency corrected  $\gamma$ -ray yields (given by their relative intensities), normalized to the  $2_1^+ \rightarrow 0_1^+$  1368.6 keV transition, are given in the last column.  $E_{level}^*$  is the energy of the initial level.